SIMULATION ANALYSIS FOR STATIC COMPRESSIVE LOAD TEST OF STEEL PIPE PILES

Kiyoka KONO[1], Shihchun LIN[2], Shuichi KAMEI[2] and Koji WATANABE[1]

[1]Department of Civil Engineering, Aichi Institute of Technology, Japan; [2]Jibanshikenjo Co., Ltd., Japan

ABSTRACT

The static load test (SLT) is highly reliable for evaluating vertical bearing characteristics, but it incurs significant expenses and extended construction time. Conversely, the rapid load test (RLT) offers advantages in terms of cost and construction time; however, it includes the impact of dynamic resistance and inertial forces of piles and ground (dynamic effects) in its data. Therefore, to accurately assess the RLT result as static vertical bearing characteristics, it is essential to remove the effect, but there are still many unresolved aspects of the mechanism of the dynamic effect, and it cannot be completely removed. In this study, both full-scale SLT and RLT for the same open-ended steel pipe test pile were carried out to compare and investigate using these vertical bearing characteristics. Therefore, as the first step, a simulation analysis using elasto-plastic FEM in the full-scale SLT and SLT results was conducted, and examined the validity of the parameter evaluation and modeling method based on the existing evaluation equations. As a result, highly reproducible results were obtained by parameter evaluation using the evaluation formula described in the design specification for highway bridges in Japan and applying the following three points: (1) joint elements simulating the shaft friction behavior obtained by the full-scale SLT, (2) consideration of soil plug effect of pile tip, and (3) a deformation modulus considering compaction effect at the deeper zone of the tip pile. Therefore, it is concluded that the parameter evaluation and modeling method are suitable for the simulation analysis of SLT.

Keywords: Static Load Test, Steel Pipe Pile, Vertical Bearing Characteristic, Elasto-plastic FEM

1. INTRODUTION

The rapid load test (RLT) offers advantages in terms of cost and construction time; however, it includes the impact of dynamic resistance and inertial forces of piles and ground (dynamic effects) in its data [1], [2]. Therefore, to accurately assess the RLT result as static vertical bearing characteristics, it is essential to remove the effect. But there are still many unresolved aspects of the mechanism of the dynamic effect, and it cannot be completely removed. In this study, both full-scale static compressive load test (SLT) and RLT for the same open-ended steel pipe test piles were carried out to compare and investigate using these vertical bearing characteristics. Therefore, as the first step, a simulation analysis using elasto-plastic FEM in the full-scale SLT and SLT results was conducted, and examined the validity of the parameter evaluation and modeling method based on the existing evaluation equations.

A flow chart of the study procedure is shown in Fig.1. In Step.2 and Step.3, determine the parameters to reproduce the SLT and RLT. This allows us to confirm that stress and deformation conditions of ground and pile, which cannot be confirmed during the test, and the mechanism of the dynamic effect is examined by comparing these parameters.

2. RESEARCH SIGNIFICANCE

SLT is highly reliable for evaluating vertical bearing characteristics, because it's carried out under the same loading conditions as actual piles. However, the test equipment requires not only force application devices and measurement devices, but also large-scale reaction systems, which incurs significant expenses and extended construction time. Conversely, RLT applies a load of short duration by free-falling a weight onto the pile head, and offers advantages in term of cost and construction time because it doesn't require reaction systems in the test equipment. However, because the data includes the impact of dynamic effects, it is essential to remove these effects to accurately evaluate the RLT results as static vertical bearing characteristics.

If the mechanism of the dynamic effect is clarified

Fig.1 A flow chart of the study

and the results obtained by RLT can be accurately analyzed as static vertical bearing characteristics, it will be possible to carry out load tests and evaluate vertical bearing characteristics more rationally.

3. FULL-SCALE SLT

3.1 Test overview

In this study, a full-scale SLT was carried out. The test pile was an open-ended steel pipe pile (SPP) of SS400 material with a pile diameter D=318.5mm, wall thickness t=6.9mm, cross-sectional area A=0.0068mm^2, pile length L=11.8m, embedment length L_d=11.0m. The pile was installed using the drop hammer method. The results of the ground investigation, pile driving depth and measurement items and locations are shown in Fig.2, and the locations of Standard penetration test (SPT) carried out at the just points and the test pile arrangement are shown in Fig.3. The measurement items were vertical displacement at the pile head (4 points), load at the pile head, and strain in each cross-section (Pile head: 4 directions, Others: 2 directions).

3.2 Load tests method

The loading method was the actual live load method using reaction piles, and loading was done in stages of 5-cycles. The planned maximum load for this test was calculated using the evaluation formula for the ultimate bearing capacity of SPP in the specifications for highway bridges (highway) construction [3]. Since the calculated ultimate bearing capacity of the test pile is R_u=751kN, the planned maximum load for the loading test is 800kN. The final loading load was set at 1040kN, which was sufficient to verify the pile's ultimate bearing capacity and other vertical bearing characteristic values that should be confirmed by loading tests, and loading was carried out at a pitch of 80kN.

4. SIMULATION ANALYSIS (SLT RESULT)

4.1 Analysis Method

4.1.1 Simulation Analysis Overview

By comparing the vertical bearing characteristics obtained from the load test results with those from the numerical analysis results, the reliability of the analysis results was confirmed, and the analytical model and ground parameters were evaluated. The analytical model and boundary conditions are shown in Fig.4. The analytical model was modeled over a quarter of the area, considering the symmetry of the test pile and the surrounding ground. The loading method was based on full-scale SLT, with 80kN applied to the pile head in stages until a maximum of

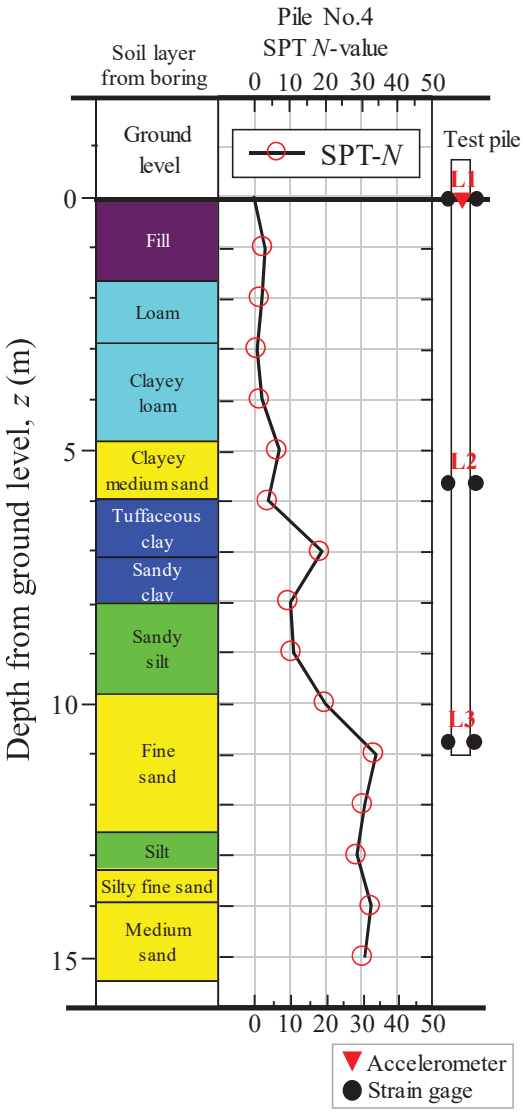

Fig.2 Profiles of soil layers, SPT N-values, together with instrumented test pile

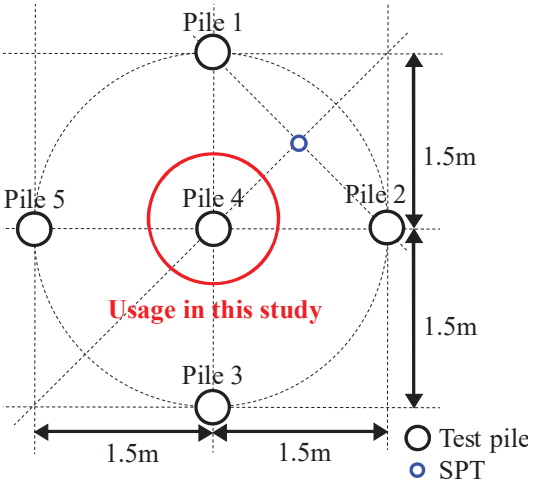

Fig.3 Locations of SPT and test piles

960kN was reached. Among the ground parameters, deformation modulus (E), cohesion (c), and internal friction angle (ϕ) were calculated in accordance with highway based on the result of previous study [4]. The Poisson's ratio was set empirically to 0.45 for clay and 0.35 for sand, and the constitutive laws were Mohr-Coulomb law for ground and elasticity for SPP.

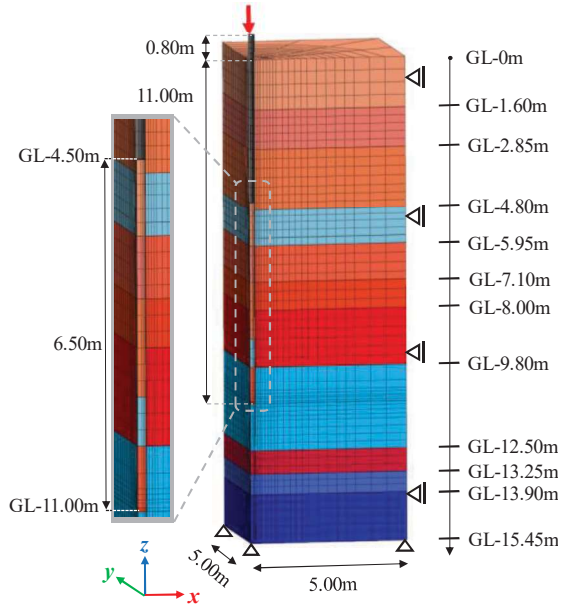

Fig.4 Analytical model and Boundary conditions

4.1.2 Assignment of Joint Elements

To simulation the shaft friction behavior between the SPP and ground, joints elements were set at the pile circumference. Shear stiffness, Normal stiffness, Cohesion, Internal friction angle, were used as joints elements parameters. Shear stiffness is based on the shaft friction – local pile displacement relationship of the full-scale SLT results, with the steeper slope adopted in the bilinear approximation. The normal stiffness was 100 times the shear stiffness, and the adhesion force of the joint element in contact with the cohesive soil was the maximum shear friction of the shaft friction per unit area - interval displacement relationship. Parameters were set in three cases (Case (A)～Case (C)) to reduce shear stiffness step by step for comparison. Table.1 lists the parameters of the set joint elements.

4.1.3 Consideration of Soilplug and Compaction

Since SPP in this study are open-ended, soilplug formed by soil that has penetrated into the pile body during driving were modeled. The soilplug set to 6.50 m, the length obtained from the full-scale SLT, as shown in Fig.4. The deformation modulus at the tip of the soilplug was set to 100 times that of the peripheral ground to account for the compaction effect associated with the driving of SPP. Also, the deformation modulus of the ground below the pile tip were changed to the average of the values obtained from highway and shear wave velocity (V_s) based on [5]. This took compaction into account for the tightening caused by the pile installation method (drop hammer method). The following is a method of calculating the deformation modulus obtained by V_s.

$$Sand: V_s = 110N^{0.3} \quad (1)$$

$$Clay: V_s = 130N^{0.29} \quad (2)$$

$$G = \rho V_s^2 \quad (3)$$

$$E = 2G(1+\nu) \quad (4)$$

where, V_s: Shear wave velocity (m/s), N: SPT N-value, G: Shear modulus (kN/m^2), ρ: Density (g/cm^3), E: Deformation modulus (kN/m^2), ν: Poisson's ratio (-)

The ground parameters used are shown in Table.2.

4.2 ANALYSIS RESULT

The axial force - displacement relationships obtained from the analysis are shown in Fig.5～7. This was calculated by multiplying the SPP strain obtained from the analysis by the elastic modulus and cross-sectional area of the steel. The axial force-displacement relationship obtained by SLT is also shown in these figures. The axial force-displacement relationship at the pile head (L1) shown in Fig.5

Table.1 Joint Element Parameters

	Case(A)		Case(B)		Case(C)	
	L1 - L2	L2 - L3	L1 - L2	L2 -L3	L1 - L2	L2 - L3
Choesion (kN/m^2)	12.38	78.29	12.38	78.29	12.38	78.29
Shear stiffness (kN/m^3)	28000	390000	6200	19000	3500	10000
Normal stiffness (kN/m^3)	2800000	39000000	620000	1900000	350000	1000000
Internal friction angle ϕ ($^\circ$)	7.2	40.23	7.2	40.23	7.2	40.23

indicates that in Case(A), the behavior in the elastic range and the axial force values at each load stage were almost identical. However, the range from the axial force at 0.01*D* to reaching the ultimate bearing capacity resulted in an overestimation of the SLT results. In Case(B) and Case(C), the values of axial force at each load stage were also almost identical. The values of axial force at the same displacement level were evaluated to be smaller as the shear stiffness decreased.

L2 is shown in Fig.6. In all cases, the axial force at 80kN loading was negative. The reason for this is that the cohesion of the joint element is taken as the maximum value of shaft friction. At the stage of loading 80kN, the shaft friction force had not yet reached its maximum value, and this exceeded the value of the axial force, which is considered to be negative. However, Case(A) in particular shows a trend like the SLT results in elastic range, and is the most appropriate parameter evaluation among the three cases. From the above, the parameter evaluation method using Case(A) is appropriate for L1 and L2.

As shown in Fig.7, at the pile tip (L3), the initial stiffness matched in all cases. For L3, we conclude that Case(C), which has the lowest shear stiffness, is optimal with a maximum axial force of 460kN, which best reproduces the SLT result of 545kN.

From the results of the above analysis, two common trends were obtained for all cross-sections and all cases.

The first is that the displacement at the same load in the plastic range is small. The reason for this is that the constitutive law of SPP is elastic and doesn't reproduce the behavior in the plastic range.

The second is that each decrease in shear stiffness reduces the initial slope at L1 and L2 and contributes to the development of axial forces at L3. Thus, different axial force-displacement relationship can be obtained by varying the shear stiffness, indicating that the shaft friction is dominant in the tip bearing capacity development mechanism of SPP.

Next, a contour diagram (Fig.8) was used to confirm the mechanics of tip bearing capacity. Since no displacement exceeding 0.1*D* was observed in all cases and all cross sections, the stress acting in the vertical direction at 960kN loading in Case (A)~Case (C) is compared as the ultimate bearing capacity. Fig.8 shows that there is no significant difference in the stress distribution in each case at 80kN loading, but there is a slight difference in the stress distribution at 480kN loading. In all cases when 960kN loading was applied, it was confirmed that the load applied to the pile head was transmitted to the tip of the pile, indicating that the bearing capacity was reliably transmitted to the tip of the pile. Especially, in Case (C), stress transmission was observed from the pile tip to a depth of about 2.5 times the pile diameter in the vertical direction.

Finally, the restrain effect of the soilplug was confirmed. If the stress acting horizontally on the soilplug is greater than the stress acting horizontally in the ground around the soilplug, it is expected to improve the adhesion to the SPP due to the restraining effect and contribute to the development of the tip bearing capacity. Horizonal stress at depth where soilplug was observed in the full-scale SLT were calculated from Equations (5) and (6) below.

Table.2 Ground Parameters

	E (kN/m^2)			c (kN/m^2)	ϕ (°)
No.	Road	Uchida.et.al (2019)	Usage date	Usage date	
1 Clay	8400	181146	8400	18.75	0.20
2 Clay	5600	146711	5600	33.73	0.20
3 Clay	5600	146711	5600	42.88	0.20
4 Sand	19600	189008	19600	10.00	25.25
5 Clay	11200	210377	11200	282.50	0.20
6 Clay	53200	440397	53200	72.50	0.20
7 Clay	30800	356001	30800	72.50	0.20
8 Sand (Pile-tip or above)	78400	466392	78400	10.00	35.49
8 Sand (Pile-tip or below)	78400	466392	233196	10.00	35.49
9 Clay	33600	372478	203039	128.25	0.20
10 Sand	78400	466392	272396	10.00	35.49
11 Sand	89600	470448	280024	10.00	36.91

$$\sigma_h = K_0 \cdot \sigma_v \quad (5)$$

$$K_0 = \nu / (1-\nu) \quad (6)$$

where, σ_h: Horizontal stress (kN/m^2), K_0: Coefficient of earth pressure at rest (-), σ_v: Overburden pressure (kN/m^2), ν: Poisson's ratio (-)

The calculated horizontal stress in the ground around the soilplug were approximately 131kN/m^2 at GL-8.90m and 152kN/m^2 around the lower end. The stress distribution at GL-8.90m from the top of the soilplug was omitted because no significant difference was observed. Fig.9 shows the horizontal stress distribution from GL-8.90m to GL-11.00m for 80kN, 480kN and 960kN loadings. When 80kN was loaded, it was confirmed that stress of 220kN/m^2 or more, which is greater than the horizontal stress acting on the peripheral ground, was acting from around GL-9.80m, which is about 1/5 of the plug length, in all cases, and a restraining effect on the soilplug was observed from the initial stages of loading. The stresses increased as the loading load was increased, and at loading load is 960kN, Case (A) was 730kN, Case (B) was 1000kN, and Case (C) was 1150kN at GL-9.80m. These stresses were 5 to 9 times greater than the stresses before loading. At GL-11.00m (tip of the soil plug), a maximum stress of 3630kN/m^2 in Case (A), 4984kN/m^2 in Case (B), and 6000kN/m^2 in Case (C), which is the largest stress among the three cases and about 40 times the stress before loading, were observed in the horizontal direction. From the above, it was confirmed that a restraining pressure acts on the soilplug from the initial stage of loading, and that this contributes to the development of the tip bearing capacity.

5. CONCLUSION

In this study, as an analytical investigation, we performed a replication analysis using elasto-plastic FEM on full-scale SLT and SLT results to examine the validity of parameter evaluations and modeling methods based on the existing evaluation equations. The findings of this study are as follows.

1) The axial force-displacement relationship at the pile head and two cross sections showed a tendency similar to the behavior of the SLT in the elastic range by the evaluation method using the parameters in Case (A).

2) In the axial force-displacement relationship at L3, the initial stiffness matched in all cases, but especially Case (C), which has the lowest shear stiffness, showed the best consistency among the three cases.

From the above, we conclude that the evaluation method using the parameters in Case (3) is the best to reproduce the behavior of the tip.

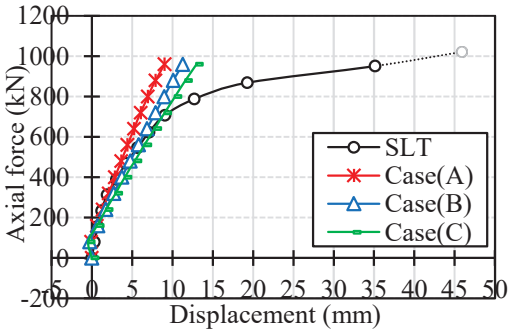

Fig.5 Axial force – displacement (L1)

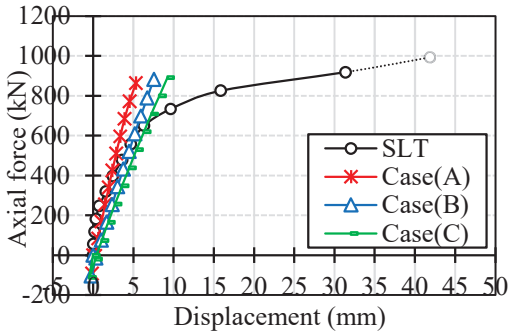

Fig.6 Axial force – displacement (L2)

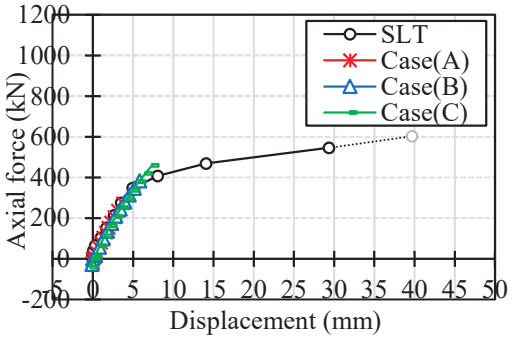

Fig.7 Axial force – displacement (L3)

3) Different axial force-displacement relationships can be obtained by varying the shear stiffness, confirming that shear friction is dominant in the mechanism of SPP bearing capacity development.

4) In all cases when 960kN load was applied, it was found that the load applied to the pile head was transmitted to the pile tip. Particularly, in Case (C), stress transmission was confirmed from the pile tip to a depth similar to about 2.5 times the pile diameter in the vertical direction.

5) The restraining effect on the soilplug was observed from the initial stage of loading from the depth of 1/5 of the plug length. Therefore, it was confirmed that the soilplug contributed to the development of the tip bearing capacity.

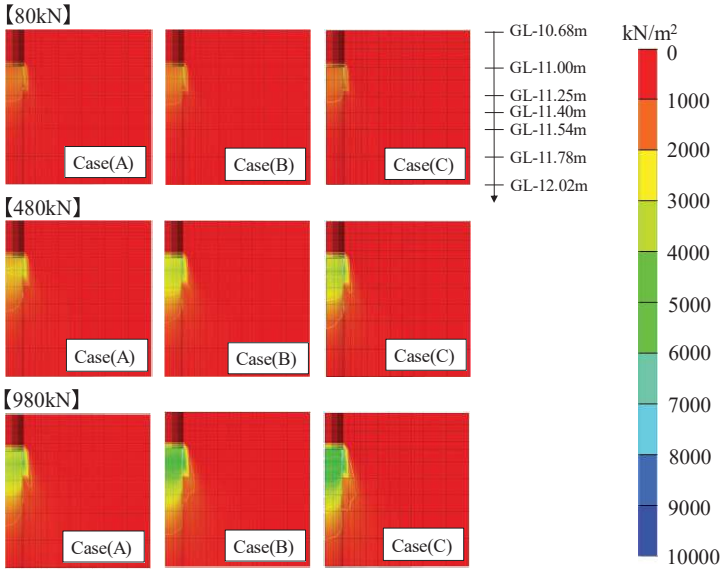

Fig.8 Distribution of vertical downward stress in each case (80kN, 480kN, 960kN)

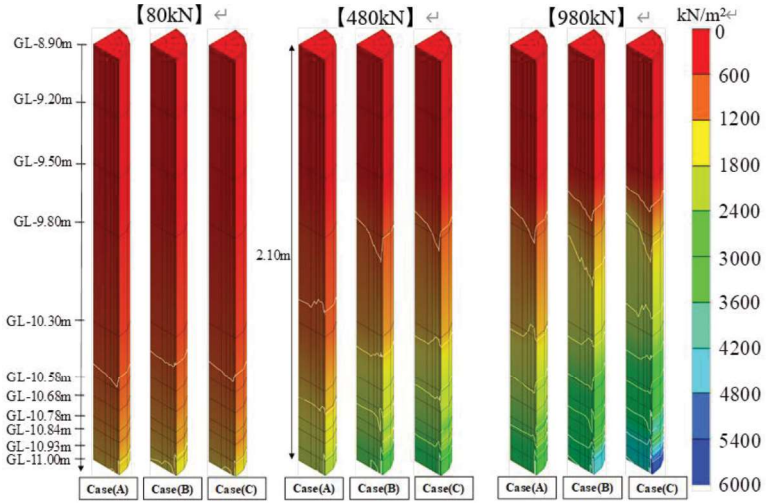

Fig.9 Horizontal stress distribution for soilplug in each case (80kN, 480kN, 960kN)

6. REFERENCES

[1] Lin S, Kamei S, Yamamoto I and Matsumoto T, Hybridnamic rapid load testing with UnLoading Point Connection method invoking Case method, Proceedings of 17th Asian Regional Conference on Soil Mechanics and Geotechnical Engineering, 2023, pp. 1425-1429.

[2] Lin S, Watanabe K, Naka Y and Matsumoto T, Load–Displacement Relations of a Driven Steel Pipe Piles from Static and Rapid Load Tests, and Empirical Formulas Based on SPT and CPT: A Case Study at Sashima Test Yard, Proceedings of the 5th International Conference on Geotechniocs for Sustainable Infrastructure Development, 2023, pp. 245-252.

[3] The specifications for highway bridges Part IV Substructures, and Part I Common, Japan Load Association, 1996.12, pp. 136-137. (in Japanese)

[4] Kono K, Lin S, Kamei S, and Watanabe K, Simulation Analysis of Compressive Load Test of Steel Pipe Piles, Proceedings of the 59th Annual Conference on Geotechnical Engineering, 2024. (in Japanese)

[5] Uchida A, Tokimatsu K, and Tsujimoto K, A study on estimation of S-wave velocity by N-value, Technical Report of the Architectural Institute of Japan, 2019.2, pp. 119-122. (in Japanese)